



RESEARCH LETTER

10.1002/2015GL065291

Special Section:

First Results from the MAVEN Mission to Mars

Key Points:

- We compared our 3-D model predictions of the hot O corona with the coronal scans taken by IUVS/MAVEN
- The transition altitude and altitude variation of hot O show good agreement with the observations
- The 3-D geographic variability of the model prediction is also seen in the IUVS coronal scans

Correspondence to:

Y. Lee,
yunilee@umich.edu

Citation:

Lee, Y., M. R. Combi, V. Tenishev, S. W. Bougher, J. Deighan, N. M. Schneider, W. E. McClintock, and B. M. Jakosky (2015), A comparison of 3-D model predictions of Mars' oxygen corona with early MAVEN IUVS observations, *Geophys. Res. Lett.*, 42, doi:10.1002/2015GL065291.

Received 15 JUL 2015

Accepted 17 SEP 2015

A comparison of 3-D model predictions of Mars' oxygen corona with early MAVEN IUVS observations

Yuni Lee¹, Michael R. Combi¹, Valeriy Tenishev¹, Stephen W. Bougher¹, Justin Deighan², Nicholas M. Schneider², William E. McClintock², and Bruce M. Jakosky²

¹Department of Atmospheric, Oceanic and Space Sciences, University of Michigan, Ann Arbor, Michigan, USA, ²Laboratory for Atmospheric and Space Physics, University of Colorado Boulder, Boulder, Colorado, USA

Abstract We have compared our 3-D hot O corona model predictions with the OI 130.4 nm emission detected by Imaging Ultraviolet Spectrograph/Mars Atmosphere and Volatile Evolution (IUVS/MAVEN) based completely on our best pre-MAVEN understanding of the 3-D structure of the thermosphere and ionosphere. The model was simulated appropriately for the observational conditions. In addition to dissociative recombination (DR) of O₂⁺, DR of CO₂⁺ is also considered as an important hot O source. The model predictions showed excellent agreement with the transition altitude, the observed altitude variation of density, and the spatial variation of the corona with respect to the Mars-Sun geometry. While previous models predicted escape rates covering a range of nearly 100, the brightness of the modeled hot O densities is a factor of ~1.5 lower than the observations. We discuss possible changes to the model that could come from further analysis of MAVEN measurements and that might close the gap between the modeled and observed brightness.

1. Introduction

Early analysis of the observations from Mariner 6, 7, and 9 suggested that Mars lost atomic oxygen to interplanetary space with the energy supplied by dissociative recombination of O₂⁺ in the exosphere [McElroy, 1972]. There have been limited observations that could confirm the hot component of O at Mars [e.g., Carveth *et al.*, 2012] until recently. See Y. Lee *et al.* (Hot oxygen corona at Mars and the photochemical escape of oxygen—Improved description of the thermosphere, ionosphere and exosphere, submitted to *Journal of Geophysical Research: Planets*, 2015) for a discussion and references therein. In 2007 the Alice UV spectrometer on board the Rosetta spacecraft made measurements of the OI 130.4 nm emissions up to high altitudes where the hot (nonthermal) O atoms are expected to dominate over the cold (thermal) O atoms [Feldman *et al.*, 2011]. Because of the orientation and movement of the instrument slit on the sky, which was not optimized to capture a Mars limb scan altitude profile, it was difficult to identify the transition altitude of the cold and hot components of atomic O (Y. Lee *et al.*, submitted manuscript, 2015). However, there was reasonable agreement of the new Y. Lee *et al.* (submitted manuscript, 2015) model brightness with the Alice observation at high altitudes.

The investigation of the photochemical escape of O has been an important subject since the loss of O is directly related to the evolution of water and CO₂ inventories at Mars. Various modeling efforts have investigated the formation and structure of the hot O corona [Cipriani *et al.*, 2007; Fox and Hać, 1997, 2009, 2014; Gröller *et al.*, 2014; Hodges, 2000, 2002; Kim *et al.*, 1998; Valeille *et al.*, 2009a, 2009b, 2010a, 2010b; Yagi *et al.*, 2012; Y. Lee *et al.*, submitted manuscript, 2015] and have provided a range of estimated escape rates. Since the escape rate cannot be directly measured by instruments, it is important to constrain the corona models thoroughly in accordance with both in situ and remote measurements of the upper thermosphere, ionosphere, and exosphere and then use the model to estimate the escape rate.

The Mars Atmosphere and Volatile Evolution (MAVEN) mission [Jakosky *et al.*, 2015] launched on 18 November 2013 was successfully inserted into orbit around Mars on 22 September 2014. MAVEN is currently exploring all aspects of the Martian upper atmosphere, composition and processes controlling atmospheric loss, as well as the solar radiation, particles, and fields driving those processes by making comprehensive measurements with its in situ and remote sensing instrument packages. The Imaging Ultraviolet Spectrograph (IUVS) on board MAVEN [McClintock *et al.*, 2014], a far UV and middle UV spectrograph, makes remote sensing measurements of the global composition and structure of the upper atmosphere, ionosphere, and corona.

We present here comparisons between 3-D model predictions of the Martian O corona and early observations taken by IUVS/MAVEN with the coronal scan mode of the instrument from 12 November 2014 to 17 January 2015. Pre-MAVEN simulations using our 3-D corona model (Y. Lee et al., submitted manuscript, 2015) are used to compute the exospheric distribution of hot O for comparison with these first IUVS coronal scans. During this observation period, Mars was moving from the solar longitude (L_s) of 231.8° to 274° , corresponding to a seasonal change from near the end of autumn to the beginning of winter for the northern hemisphere (near perihelion). Solar activity is estimated as solar moderate conditions ($F_{10.7} \approx 130$). This indicates that our solar moderate perihelion case (Y. Lee et al., submitted manuscript, 2015) is appropriate for comparisons.

Coronal scans by IUVS are performed along the outbound orbit, while the instrument points toward the inbound leg—more details of the IUVS coronal scan data used here are described in the paper *Deighan et al.* [2015]. The OI 130.4 nm emission intensity was measured over a range of viewing geometries including the night-to-day and day-to-night look directions, where most of the dayside exosphere was measured in various directions from the upper thermosphere to nearly 3000 km altitude. Particularly, the slit, oriented parallel to orbit normal, is favorable for precise observations of the optically thin (at high altitudes) and thick (at lower altitudes) oxygen. The two-component structure of exospheric O allowed us to decompose the brightness profiles from IUVS into two separate OI 130.4 nm contributions, which led to estimation of the transition altitude, validating the model estimation.

2. Modeling of the Hot O Corona: The 3-D Coupled Framework of Mars-AMPS and M-GITM

The Martian O corona is simulated by Mars application of the 3-D Adaptive Mesh Particle Simulator (M-AMPS) coupled with the 3-D Mars Global Ionosphere Thermosphere Model (M-GITM). The AMPS code [*Tenishev et al.*, 2008, 2013] is a kinetic particle model developed within the Direct Simulation Monte Carlo [*Bird*, 1994] method. AMPS solves a wide range of kinetic problems by representing the collisional dynamics of an ensemble of model particles. Coupled with the Mars exospheric code, AMPS captures the physics of the hot particle distribution in the Martian upper atmosphere. The modeling of the Martian hot corona requires the M-AMPS code to run in a test particle Monte Carlo mode. A more detailed description of M-AMPS can be found in comprehensive studies of the Martian hot C corona [*Lee et al.*, 2014a, 2014b] and hot O corona (Y. Lee et al., submitted manuscript, 2015).

M-GITM [*Bougher et al.*, 2015] is based on the Earth GITM code [*Ridley et al.*, 2006], and is a newly developed Martian thermosphere and ionosphere model. M-GITM solves the self-consistent finite difference primitive equations for the time-dependent thermosphere and ionosphere without the hydrostatic assumption. Here the formulations and subroutines have largely been taken from the NASA Ames' Mars general circulation model [e.g., *Haberle et al.*, 1999] and National Center for Atmospheric Research Mars thermosphere general circulation model [e.g., *Bougher et al.*, 2008] codes. A single treatment of the whole Martian atmosphere from the surface to the exosphere (0–300 km) ensures inclusion of dynamical coupling processes linking the lower and upper atmosphere.

M-GITM provides the densities of the thermospheric and ionospheric species (O, CO₂, CO, N₂, O₂⁺, CO₂⁺, and e⁻), temperatures (T_e , T_n , and T_i), and three components of neutral winds as input to the M-AMPS code from ~100 km to ~250 km. The production and thermalization of hot O in M-AMPS are controlled according to the source and collisional background atmosphere supplied by M-GITM. Details of the background atmosphere and its solar cycle and seasonal variabilities for the hot O corona study are given in Y. Lee et al. (submitted manuscript, 2015).

In the simulation, the energy of a nascent hot O atom is modified by collisions with the ambient thermospheric constituents as it travels under the gravitational influence of the planet. Our approach includes a total of four thermospheric species, O, CO₂, CO, and N₂, as collision partners for the hot O atoms. The collisions between hot O and thermal species are described realistically by adopting a forward scattering collision scheme and using the angular differential cross sections computed by *Kharchenko et al.* [2000]. The same angular dependency of the cross sections is applied for all hot O collisions with different integrated total cross

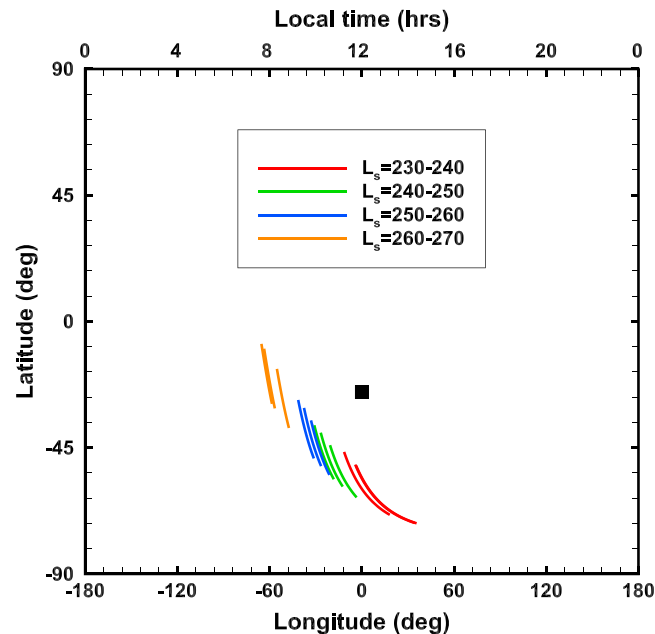


Figure 1. Positions of IUVS/MAVEN in the model time frame (the lines of sight are not shown). The subsolar point is indicated as a black square. The colors of the spacecraft trajectories correspond to the same colors of the solar longitude (L_s) ranges.

(^3P) channel with $\sim 100.0\%$ branching ratio, the energy distribution of nascent hot O is highly concentrated at energies between ~ 4.8 eV and ~ 5.7 eV. According to the O_2^+ and CO_2^+ DR rates, the maximum production of hot O occurs around the subsolar region, while no hot O is produced on the nightside. A hot particle is considered to be thermalized and removed from the simulation when the velocity of the particle falls below a threshold velocity ($V_{\text{threshold}} = 2 \times \text{local thermal speed}$). The nonnegligible contribution from secondary hot O atoms, which can be produced from the energy transfer from hot O to thermal O [Valeille *et al.*, 2010a; Y. Lee *et al.*, submitted manuscript, 2015], is also taken into account.

3. Results: Comparisons of the 3-D Model Predictions With the IUVS/MAVEN Observations

We selected 12 orbits from the nominal coronal scan data set described in Deighan *et al.* [2015], which are Planetary Data System products with identifier v02_r01, for comparison with the model. It is important to note that IUVS was calibrated against UV bright stars, scaled by instrument geometric factors appropriate for extended source observations [Schneider *et al.*, 2015]. The measurement details and basic analysis of the corona observations are explained by Deighan *et al.* [2015].

As mentioned above, we adopted our appropriate perihelion and solar moderate case ($L_s = 270^\circ$ and $F_{10.7} = 130$) (Y. Lee *et al.*, submitted manuscript, 2015) for all comparisons shown in this study. The observations were taken when the planet was moving toward perihelion during moderate solar activity, where the change in L_s was $\sim 40^\circ$. Although the thermosphere and ionosphere constantly change over the observation time period, we assumed that deviations from the actual atmospheric conditions are not significant. The hot O corona was simulated with an upper boundary of $6 R_M$ from the center of the planet. A particular universal time (UT) is chosen from M-GITM, allowing the subsolar point to be located approximately at 0° longitude and -25.19° latitude.

The position and look direction of the instrument were adjusted to the model time frame by applying a transformation matrix for each integration period. As shown in Figure 1, the spatial locations are distributed over a wide range of latitude and local time on the dayside. The locations where the limb scans were taken change from the dusk region on the southern hemisphere to the equator near the dawn terminator on the dayside of the corona. The density of the simulated hot O corona was integrated in the model frame along the lines of sight of IUVS and converted to OI 130.4 nm emission brightness assuming an optically thin g

sections assumed for each collision pair. Due to the small collision frequency, the collisions between hot O atoms are safely disregarded.

The fate of the hot particles within the computational domain and thus the structure of the hot corona are determined by the local variations of the sources and the physical conditions in the atmosphere. In addition to dissociative recombination (DR) of O_2^+ , which is a major source of hot O that is widely accepted by previous studies, we also considered DR of CO_2^+ as an important source of hot O for this study. Gröller *et al.* [2014] first examined the potential of DR of CO_2^+ in hot O production and concluded that DR of CO_2^+ is also a major source of hot O. In our 3-D coupled framework, we also found that the contribution of DR of CO_2^+ to the total hot O content is comparable to that of DR of O_2^+ . Due to the large excessive energy from the $\text{CO}(^1\Sigma)+\text{O}$

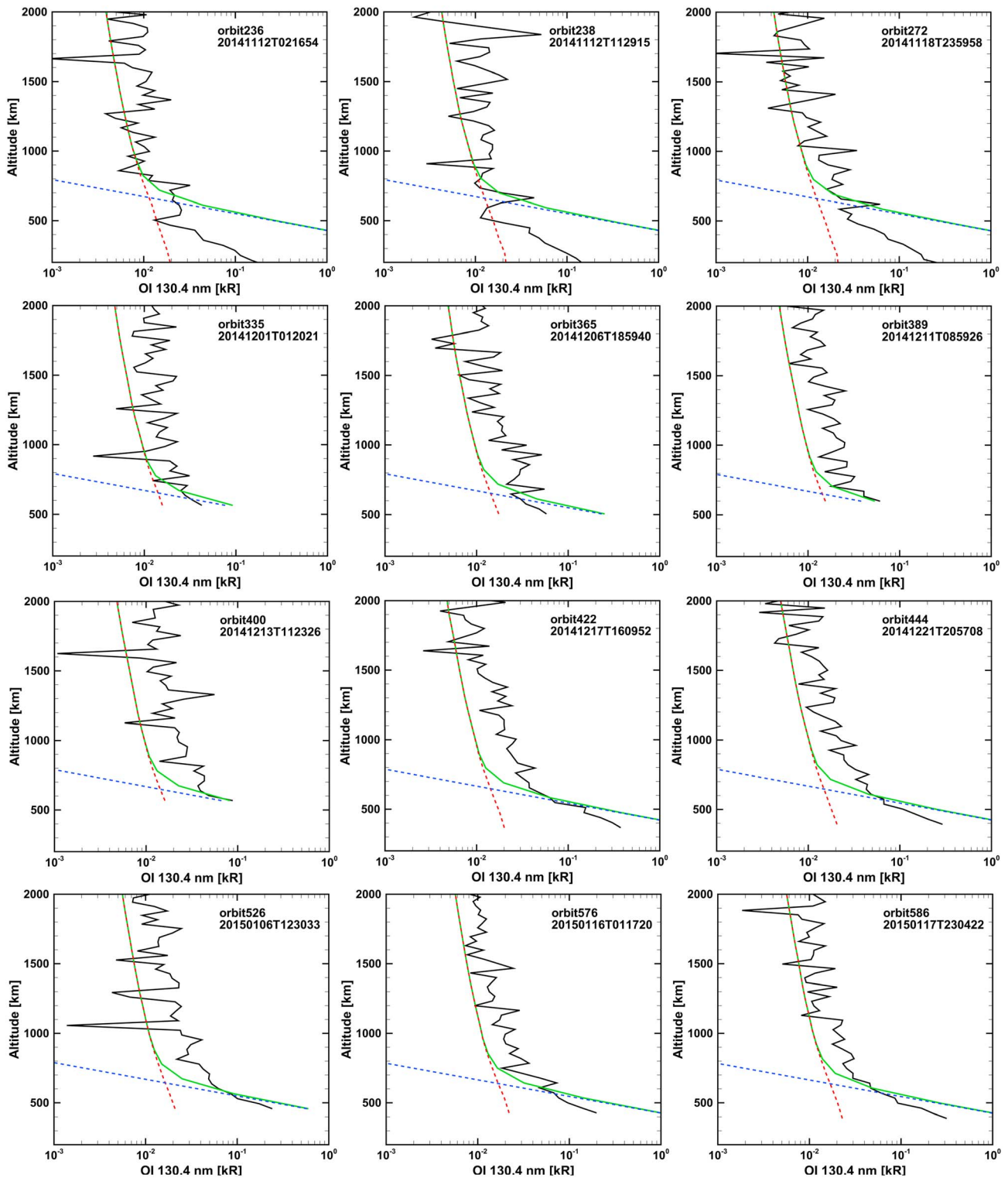


Figure 2. Comparisons of the modeled OI 130.4 nm brightness from the simulation by the Mars-AMPS and M-GITM coupled framework with the IUVS/MAVEN coronal limb scan data for a selected set of orbits during a time period from 12 November 2014 to 17 January 2015 [Deighan et al., 2015]. The black solid curves indicate the IUVS observations. The model prediction of total exospheric O brightness is shown by the green solid curves, which are decomposed into the hot (red dash) and cold (blue dash) components in each plot. The estimated transition altitude by the model is approximately where the blue and red curves are crossed.

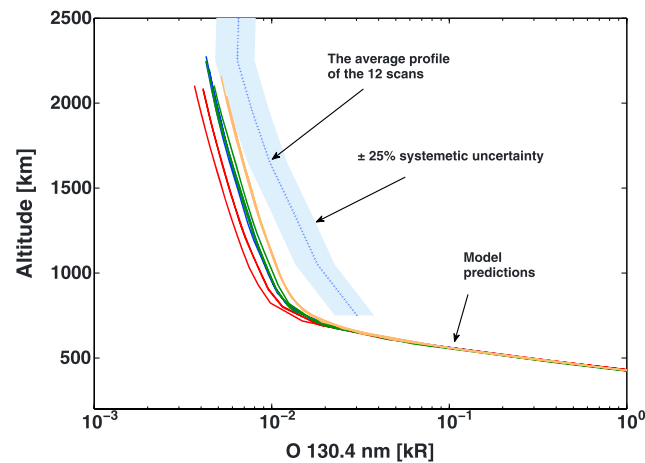


Figure 3. Average OI 130.4 nm brightness profiles from the model and observations. The blue shaded region shows the systematic uncertainty of $\pm 25\%$. The blue dash line indicates the average profile of the 12 scans. All solid lines are the corresponding 12 brightness profiles predicted by the model. The color of the model profiles matches the color in Figure 1.

emission intensities. The observed brightness becomes abruptly larger by about an order of magnitude at low altitude, which appears as the two scale heights for exospheric O. Compared to the previous hot O coronal observations by Alice/Rosetta [Feldman *et al.*, 2011], which were not optimal for determining the limb column distribution, a substantially slower decrease in brightness with increasing altitude is found over all the orbits considered in this study as is a more abrupt transition from the hot O to cold O. As mentioned, a more detailed comparison between our model predictions and the Alice observations is discussed by Y. Lee *et al.* (submitted manuscript, 2015). At higher altitudes (~ 1200 km) the model calculations agreed quite well with the Alice observations.

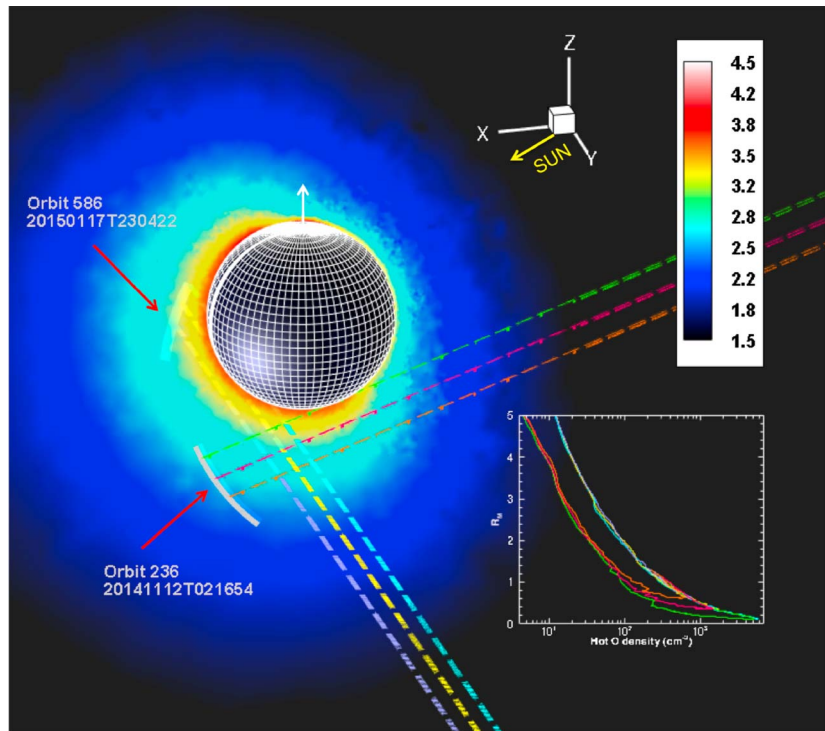
As shown in Figure 2, our model calculations show reasonable agreement with the observations, considering the $\pm 25\%$ systematic uncertainty associated with the calibration. The variation with altitude is quite consistent between model and measurements indicating that the modeled hot O temperatures (a few thousand kelvins) are correct. Since the hot O density is the final product from our coupled framework, the cold and hot O contributions were separately obtained from M-GITM and M-AMPS. The transition altitude is estimated to be ~ 650 km, which is located where the brightness profiles of the hot and cold components intersect. At altitudes below ~ 400 km, the discrepancies between model and observed brightness become considerably larger, where the cold O becomes optically thick. At limb altitudes lower than ~ 600 km (below transition altitude), the hot O merges with cold O. This is consistent between model and data. As a consequence, our models overestimate the O brightness in the lower atmosphere, where cold O dominates over hot O. However, at high altitudes, where hot O is a dominant component, the combination of low column densities and high temperatures of hot O is consistent with the optically thin assumption.

Figure 3 shows a comparison of the average of all 12 coronal scans chosen for this study with all of the individual model predictions. The 12 coronal scans are averaged over 300 km altitude intervals to remove the local time variation and the noise in the data. The range between the minimum and maximum values for the average profile obtained from the observations is shown as a shaded area, which indicates the systematic uncertainty of $\pm 25\%$, to give the plausible range of the O brightness. The range of the model predictions from the geographic variation encompasses the minimum values of the measured average profile at high altitudes. Clearly, the altitude variation of the models is in excellent agreement with that in the IUVS measurements.

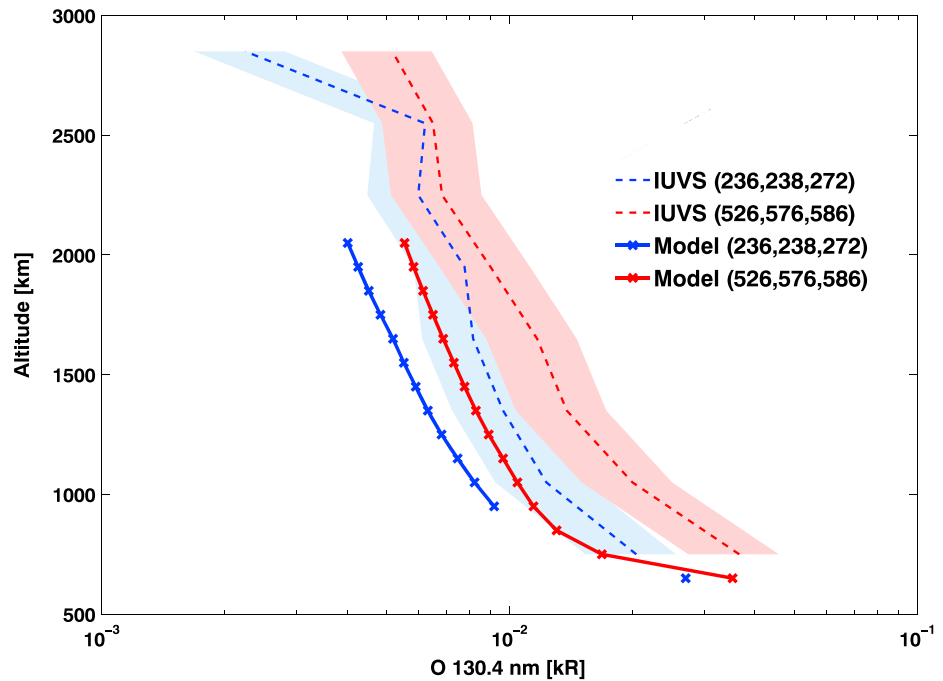
Because the individual observations were taken with different geometries and viewing different regions of the dayside corona, the structural differences in the hot O corona should be evident in the observed OI 130.4 nm emissions. The spatial variation of the hot O corona can be observed by taking advantage of the large local time coverage of the coronal scan set. According to the observation geometry (Figure 1), the first and last coronal scans considered in this study were taken in the afternoon and near the dawn equatorial region, respectively.

factor of $5.74 \times 10^{-6} \text{ s}^{-1}$. In order to estimate the transition altitude, we carried out a separate computation of cold O brightness profiles utilizing thermal O from M-GITM, but the optically thin approximation begins to fail below about 600 km.

Figure 2 shows the comparisons between the IUVS observations and the total exospheric O (i.e., hot O and cold O) brightness predicted by the models. The 12 scans are organized by L_s of Mars, where, from the top to bottom, each row corresponds to the L_s range of $230^\circ\text{--}240^\circ$, $240^\circ\text{--}250^\circ$, $250^\circ\text{--}260^\circ$, and $260^\circ\text{--}270^\circ$, respectively (refer to Figure 1 for the spatial information of the individual profiles). Wave-like irregular oscillations at high altitudes are most likely simply due to noise from the low



(a)



(b)

Figure 4. Geographic variation in the hot O corona. (a) Three-dimensional view of spacecraft trajectories during orbits 236 and 586 when IUVS was measuring the OI 130.4 nm emission. The dash lines show several lines of sight of the instrument. The background color contour shows the \log_{10} of density of the hot O corona in units of cm^{-3} . The bottom right panel shows the extracted hot O density profiles along the lines of sight. The colors of the profiles match those of the lines of sight. (b) Average profiles for the first (blue) and last (red) three coronal scans (first three: orbits 236, 238, and 272 and last three: orbits 526, 576, and 586) calculated from the model and observations. The model predictions are the lines with crosses. The shaded regions show the systematic uncertainty based on the IUVS calibration.

As described earlier, the hot O corona is not spherically symmetric around the planet (Y. Lee et al., submitted manuscript, 2015). The structure of the hot corona is strongly correlated with the characteristics of the thermosphere and ionosphere. The local variation of the hot O production is first determined by the spatial distribution of the sources and modified by the local collision partners and other atmospheric conditions, which allows the model to capture the complicated 3-D nature of the hot corona.

Figure 4a shows several lines of sight of the instrument for the first and last few coronal scans in the data set. During the first coronal scan, the look direction of the instrument was oriented directly toward the nightside, integrating through high-latitude regions of the corona. For the last coronal scan, the corona was observed from the low to high latitude, where a much wider area of the corona across the dawn region was included in the column integration than that of the first scan. The difference in the corona observed during these two scans is shown in the extracted hot O density (the bottom right panel in Figure 4a). The hot O corona densities were extracted along the instrument's lines of sight from our simulation up to the upper boundary of our computational domain ($\sim 5 R_M$ altitude). Our model predicted that the difference in the hot O densities seen by these two coronal scans is a factor of ~ 2.5 . This difference is reached when the density profiles for the first scan begins deviating from those for the last scan with increasing distance from the day-night terminator. Since the brightness is directly related to the density, which is the integrand in the brightness calculation, it is expected that the resulting O brightness profiles also display a similar difference for these two scans.

Due to large fluctuations in the individual measured profiles, the coronal scans that have similar observational geometry were averaged together to average out the noise for a better comparison (i.e., Figure 2 (first and fourth rows) are averaged separately). Figure 4b shows the two averaged O profiles from IUVS with the systematic uncertainty plotted with those representing the average of the corresponding set of model predictions. Despite the overall magnitude difference between the modeled and measurement O brightness, it is clearly shown that the difference observed because of the geographic variation is seen in the measurements and is consistent with that predicted by the model simulation.

4. Conclusion

MAVEN IUVS made coronal scans of the OI 130.4 nm brightness over a range of viewing geometries from the upper thermosphere to ~ 3000 km altitude. We compared our pre-MAVEN model predictions with the 12 coronal scans that were chosen for this study. The spatial locations, where the integrations are performed for each scan, cover a wide range of local time and latitude of the dayside hot O corona.

Several aspects of the model compare very favorably to the new MAVEN data, namely, (1) the variation of hot O density with altitude above 600 km, (2) the day-night distribution of the hot O density, and (3) the transition altitude from hot O in the corona to cold O in the upper thermosphere. The consistency of the altitude variation means that the temperature of the hot O corona (a few thousand kelvins) is well matched by the observation. Our model simulation showed that the contribution of DR of CO_2^+ to the total hot O density is comparable to that of DR of O_2^+ . The resulting hot O corona in combination of both reactions showed better agreement with the observations than the case that considers DR of O_2^+ only. The escape of hot O from DR of CO_2^+ is less likely to be regulated by the background atmosphere due to the large velocity of nascent hot O than the hot O from DR of O_2^+ . The overall brightness of the hot O corona observed by IUVS is, however, a factor of ~ 1.5 larger than the pre-MAVEN model. As discussed by Y. Lee et al. (submitted manuscript, 2015), previous models of the hot O corona and escape cover a range of nearly 100 in predicted escape rates. Many previous models of the escape rate did not, however, calculate a hot corona density distribution, but as there is a direct correlation between hot O densities in the corona with the escape rate, there would also be a large range in predicted corona densities based on past modeling studies.

As more MAVEN measurements are made and become available, we will test various M-AMPS model assumptions and the M-GITM model results that are M-AMPS inputs to see if the difference can be resolved. One contribution to hot O in the corona, which should not be large enough by itself but might contribute, could be sputtering of neutral cold O by impact from mainly O^+ pickup ions [Luhmann and Kozyra, 1991; Johnson and Luhmann, 1998]. Otherwise, the major model inputs that come into play are (1) the hot O source, namely, the O_2^+ and electron density and temperature distributions and (2) the collision cross sections and the density distributions of the major atmospheric species that regulate the amount of nascent hot O that enters the corona and some of which that

eventually escapes. Fortunately, data taken by the MAVEN mission and to be taken in the coming months and years will enable us to constrain nearly all of them. Finally, our pre-MAVEN model calculation predicts a neutral hot O escape rate for solar moderate and perihelion conditions of 9.1×10^{25} O atoms s^{-1} , where the contribution of DR of CO_2^+ is $\sim 62\%$ of the total. Based on previous model calculations, which expect a positive correlation between coronal density and escape rate [Vaille et al., 2009b; Y. Lee et al., submitted manuscript, 2015], the model-IUVS data difference would imply a total escape rate of $\sim 10^{26}$ O atoms s^{-1} .

Acknowledgments

This work has been supported by the MAVEN Participating Scientist grant NNX13AO27G. S.W. Bougher is supported as a MAVEN Co-I under subcontract with the University of Colorado. The MAVEN project is supported by NASA through the Mars Exploration Program. Resources for all simulations in this work have been provided by NASA High-End Computing Capability (HECC) project at NASA Advanced Supercomputing (NAS) Division. Simulation data are available upon request from the author. The M-GITM used in this study is available from MAVEN Science Data Center (<https://lasp.colorado.edu/maven/sdc/public/pages/models.html>). The data used are archived in the Planetary Atmospheres Node of the Planetary Data System.

The Editor thanks two anonymous reviewers for their assistance in evaluating this paper.

References

- Bird, G. A. (1994), *Molecular Gas Dynamics and the Direct Simulation of Gas Flows*, Clarendon Press, Oxford.
- Bougher, S. W., P.-L. Blelly, M. Combi, J. L. Fox, I. Mueller-Wodarg, A. Ridley, and R. G. Roble (2008), Neutral upper atmosphere and ionosphere modeling, *Space Sci. Rev.*, *139*, 107–141, doi:10.1007/s11214-008-9401-9.
- Bougher, S. W., D. Pawlowski, J. M. Bell, S. Nelli, T. McDunn, J. R. Murphy, M. Chizek, and A. Ridley (2015), Mars Global Ionosphere Thermosphere Model (M-GITM): Solar cycle, seasonal, and diurnal variations of the upper atmosphere, *J. Geophys. Res. Planets*, *120*, 311–342, doi:10.1002/2014JE004715.
- Carveth, C., J. Clarke, J. Chaufray, and J. Bertaux (2012), Analysis of HST spatial profiles of oxygen airglow from Mars, 44th Division for Planetary Sciences meeting, #214.03, Reno, Nevada, 14–19 Oct.
- Cipriani, F., F. Leblanc, and J. J. Berthelier (2007), Martian corona: Nonthermal sources of hot heavy species, *J. Geophys. Res.*, *112*, E07001, doi:10.1029/2006JE002818.
- Deighan, J., et al. (2015), MAVEN IUVS observation of the hot oxygen corona at Mars, *Geophys. Res. Lett.*, *42*, doi:10.1002/2015GL065487.
- Feldman, P. D., et al. (2011), Rosetta-Alice observations of exospheric hydrogen and oxygen on Mars, *Icarus*, *214*, 394–399, doi:10.1016/j.icarus.2011.06.013.
- Fox, J. L., and A. B. Hać (1997), Spectrum of hot O at the exobases of the terrestrial planets, *J. Geophys. Res.*, *102*, 24,005–24,011, doi:10.1029/97JA02089.
- Fox, J. L., and A. B. Hać (2009), Photochemical escape of oxygen from Mars: A comparison of the exobase approximation to a Monte Carlo method, *Icarus*, *204*, 527–544, doi:10.1016/j.icarus.2009.07.005.
- Fox, J. L., and A. B. Hać (2014), The escape of O from Mars: Sensitivity to the elastic cross sections, *Icarus*, *228*, 375–385, doi:10.1016/j.icarus.2013.10.014.
- Gröller, H., H. Lichtegger, H. Lammer, and V. I. Shematovich (2014), Hot oxygen and carbon escape from the Martian atmosphere, *Planet. Space Sci.*, *98*, 93–105.
- Haberle, R. M., M. M. Joshi, J. R. Murphy, J. R. Barnes, J. T. Schofield, G. Wilson, M. Lopez-Valverde, J. L. Hollingsworth, A. F. C. Bridger, and J. Schaeffer (1999), General circulation model simulations of the Mars Pathfinder atmospheric structure investigation/meteorology data, *J. Geophys. Res.*, *104*, 8957–8974, doi:10.1029/1998JE900040.
- Hodges, R. R. (2000), Distributions of hot oxygen for Venus and Mars, *J. Geophys. Res.*, *105*, 6971–6981, doi:10.1029/1999JE001138.
- Hodges, R. R. (2002), The rate of loss of water from Mars, *Geophys. Res. Lett.*, *29*(3), 1038, doi:10.1029/2001GL013853.
- Jakosky, B., et al. (2015), The 2013 Mars Atmosphere and Volatile Evolution (MAVEN) mission to Mars, *Space Sci. Rev.*, doi:10.1007/s11214-015-0139-x.
- Johnson, R. E., and J. G. Luhmann (1998), Sputter contribution to the atmospheric corona on Mars, *J. Geophys. Res.*, *103*, 3649–3653, doi:10.1029/97JE03266.
- Kharchenko, V., A. Dalgarno, B. Zygelman, and J.-H. Yee (2000), Energy transfer in collisions of oxygen atoms in the terrestrial atmosphere, *J. Geophys. Res.*, *105*(A11), 24,899–24,906, doi:10.1029/2000JA000085.
- Kim, J., A. F. Nagy, J. L. Fox, and T. E. Cravens (1998), Solar cycle variability of hot oxygen atoms at Mars, *J. Geophys. Res.*, *103*, 29,339–29,342, doi:10.1029/98JA02727.
- Lee, Y., M. R. Combi, V. Tenishev, and S. W. Bougher (2014a), Hot carbon corona in Mars' upper thermosphere and exosphere: 1. Mechanisms and structure of the hot corona for low solar activity at equinox, *J. Geophys. Res. Planets*, *119*, doi:10.1002/2013JE004552.
- Lee, Y., M. R. Combi, V. Tenishev, and S. W. Bougher (2014b), Hot carbon corona in Mars' upper thermosphere and exosphere: 2. Solar cycle and seasonal variability, *J. Geophys. Res. Planets*, *119*, 2487–2509, doi:10.1002/2014JE004669.
- Luhmann, J. G., and J. U. Kozyra (1991), Dayside pickup oxygen ion precipitation at Venus and Mars: Spatial distributions, energy deposition and consequences, *J. Geophys. Res.*, *96*, 5457–5467, doi:10.1029/90JA01753.
- McClintock, W. E., N. M. Schneider, G. M. Holsclaw, A. C. Hoskins, I. Stewart, J. Deighan, J. T. Clarke, F. Montmessin, and R. V. Yelle (2014), The Imaging Ultraviolet Spectrograph (IUVS) for the MAVEN mission, *Space Sci. Rev.*, doi:10.1007/s11214-014-0098-7.
- McElroy, M. B. (1972), Mars: An evolving atmosphere, *Science*, *175*, 443–445.
- Ridley, A. J., Y. Deng, and G. Tóth (2006), The global ionosphere–thermosphere model, *J. Atmos. Sol. Terr. Phys.*, *68*, 8, doi:10.1016/j.jastp.2006.01.008.
- Schneider, N. M., et al. (2015), MAVEN IUVS observations of the aftermath of the Comet Siding Spring meteor shower on Mars, *Geophys. Res. Lett.*, *42*, 755–4761, doi:10.1002/2015GL063863.
- Tenishev, V., M. R. Combi, and B. Davidsson (2008), A global kinetic model for cometary comae: The evolution of the coma of the Rosetta target comet Churyumov–Gerasimenko throughout the mission, *Astrophys. J.*, *685*, 659–677.
- Tenishev, V., M. Rubin, O. J. Tucker, M. R. Combi, and M. Sarantos (2013), Kinetic modeling of sodium in the lunar exosphere, *Icarus*, *226*, 1538–1549, doi:10.1016/j.icarus.2013.08.021.
- Vaille, A., M. R. Combi, S. W. Bougher, V. Tenishev, and A. F. Nagy (2009a), Three-dimensional study of Mars upper thermosphere/ionosphere and hot oxygen corona: 2. Solar cycle, seasonal variations, and evolution over history, *J. Geophys. Res.*, *114*, E11006, doi:10.1029/2009JE003389.
- Vaille, A., V. Tenishev, S. W. Bougher, M. R. Combi, and A. F. Nagy (2009b), Three-dimensional study of Mars upper thermosphere/ionosphere and hot oxygen corona: 1. General description and results at equinox for solar low conditions, *J. Geophys. Res.*, *114*, E11005, doi:10.1029/2009JE003388.
- Vaille, A., M. R. Combi, V. Tenishev, S. W. Bougher, and A. F. Nagy (2010a), A study of suprathermal oxygen atoms in Mars upper thermosphere and exosphere over the range of limiting conditions, *Icarus*, *206*, 18–27, doi:10.1016/j.icarus.2008.08.018.
- Vaille, A., M. R. Combi, V. Tenishev, S. W. Bougher, and A. F. Nagy (2010b), Water loss and evolution of the upper atmosphere and exosphere over Martian history, *Icarus*, *206*, 28–39, doi:10.1016/j.icarus.2009.04.036.
- Yagi, M., F. Leblanc, J. Y. Chaufray, F. Gonzalez-Galindo, S. Hess, and R. Modolo (2012), Mars exospheric thermal and non-thermal components: Seasonal and local variations, *Icarus*, *221*, 682–693.